Morphology and Thermal Behavior of Self-Assembling Carbamates

Mohammad Moniruzzaman, Bruce Goodbrand,† and Pudupadi R. Sundararajan*

Department of Chemistry, Carleton University, 1125 Colonel By Drive, Ottawa, Ontario K1S 5B6, Canada

Received: May 14, 2003

Hydrogen bond mediated self-assembling carbamates with alkyl side chains of different lengths were investigated with respect to thermal behavior and morphology. The length of the side chain has an influence on the heat of fusion, crystallinity, and crystallite size. Morphologies of samples slowly cooled from the melt and those quenched were different. While plasticizers or clarifiers are usually used to modify the crystalline morphology of materials, we examined the possibility of effecting similar changes by blending any two types of carbamates. Although both the heat of fusion and crystallinity decrease initially with the addition of the second component, they recover beyond a certain composition. The spherulite size also decreases significantly, enhancing the transparency of the sample. Thermal analysis shows that the components of the blend exercise a mutual plasticizer effect, reducing the melting temperatures. The changes in morphology upon blending are not due to a decrease in the extent of hydrogen bonding but can be attributed to the disorder in the packing of the alkyl side chains.

Introduction

Carbamates are an important class of compounds due to their potential scientific and technological applications. They can be used for increasing the abrasion resistance of polyurethane compositions,[1] improving the hardness of urethane-based adhesives and sealants,[2] and adjusting viscosity values of oils and greases when used as additives.[3,4] Some carbamates and thiocarbamates have biological activity and can be utilized as insecticides.[5] The association process in carbamates is similar to the biological self-assembly (e.g., protein molecules) involving hydrogen bonding. Their melt viscosity is usually of the order of a few centipoise, and they crystallize rapidly. Hence, carbamates with alkyl side chains have potential applications as vehicles in reprography and ink jet printing technologies.[6−8]

Furer computed the dynamic and electrooptical parameters (EOPs) of carbamates by the MINDO/3 method.[9] He reported an extensive study on the hydrogen bonding and IR spectra of different carbamates in conjunction with quantum-chemical calculations that can provide a probe of the actual conformations and associates present in the different phases of carbamates.[10−12] Deetz et al.[13] used hydrogen bonding templates to control the syn−anti C−N rotamer equilibrium in pyridyl carbamates, leading to an effective "conformational switch". Krol et al.[14] utilized X-ray diffraction and thermal analysis to investigate the structure and properties of some short chain mono- and dicarbamates as model compounds for urethane polymers. They found that carbamates, which were single compounds, developed their crystal structures far better than mixtures of the two isomers did. The thermal stability of monocarbamates was found to be higher than that of dicarbamates obtained from the same alcohol.

As mentioned above, due to the low melt viscosity and semicrystalline nature, long-chain monocarbamates are attractive candidates for printing applications.[6−8] For example, they can be used as a vehicle in ink formulation for ink-jet printers. In such applications, the vehicle should crystallize with high transparency and should be crease resistant. The average size of the spherulites upon crystallization should be of the order of the wavelength of light to impart transparency. Such small spherulites also increase the crease resistance. The crystalline morphology of the vehicle thus becomes an important attribute.

The purpose of this study was to investigate the thermal behavior and morphology of some long-chain monocarbamates having alkyl side chains of different length. It is a common practice in industry to incorporate plasticizers or clarifiers as nucleating agents to control the crystallinity, and spherulites size, and improve the optical properties of materials. In this paper, we attempted to control the morphology, by blending two homologous carbamates with different compositions. The difference between the use of the clarifiers and the blends as studied here is that the latter involves a homologous series of molecules. Since the self-assembling process in the carbamates is facilitated by N−H···O═C hydrogen bonding, it is of interest to study the extent to which the self-assembly would be interrupted by blending a second component. When used in the printing process, naturally the melt will be quenched instantly upon transfer to the substrate. Hence, the differences in morphology behavior between samples slowly cooled and quenched from the melt were also investigated in this study.

SCHEME 1: Preparation of Carbamates

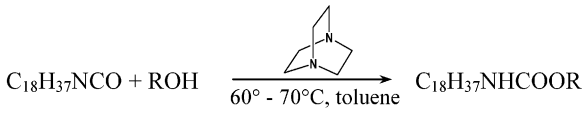

Experimental Section

Synthesis of the Carbamates. The carbamates were synthesized by reactions of Octadecyl isocyanate with 1-butanol, 1-heptanol, 1-octanol, 1-dodecanol, 1-hexadecanol, and 1-octadecanol. Reactions between the isocyanate and the suitable alcohol were carried out in toluene solution, at 60−70 °C for 2 h (Scheme 1).

* Corresponding author. E-mail: Sundar@carleton.ca.
† Xerox Research Centre of Canada, 2600 Speakman Drive, Mississauga, Ontario L5K 2L1, Canada.

10.1021/jp035336k CCC: $25.00
Published on Web 07/10/2003

TABLE 1: Carbamates Obtained from Reactions of Octadecyl Isocyanate with Different Alcohols

parent alcohol	carbamate ID	*N*-octadecylcarbamate	formula	length of the molecule,[a] Å	T_m obtained with DSC, °C
1-butanol	C_4	butyl ester	$C_{18}H_{37}(NHCOO)C_4H_9$	30.02	61.2
1-heptanol	C_7	heptyl ester	$C_{18}H_{37}(NHCOO)C_7H_{15}$	33.98	65.5
1-octanol	C_8	octyl ester	$C_{18}H_{37}(NHCOO)C_8H_{17}$	35.19	66.0
1-dodecanol	C_{12}	dodecyl ester	$C_{18}H_{37}(NHCOO)C_{12}H_{25}$	40.39	72.8
1-hexadecanol	C_{16}	hexadecyl ester	$C_{18}H_{37}(NHCOO)C_{16}H_{33}$	45.44	83.0
1-octadecanol	C_{18}	octadecyl ester	$C_{18}H_{37}(NHCOO)C_{18}H_{37}$	47.99	86.5

[a] Calculated by using HyperChem Pro 6 molecular visualization and simulation software (Hypercube Inc.).

1,4-Diazabicyclo[2.2.2]octane (DABCO) was used as the catalyst. All the reagents were purchased from Aldrich. The reaction products were purified by recrystallization and were confirmed by IR and NMR. The carbamates that were synthesized are listed in Table 1with the samples identified as C_X, which stands for the carbamate having X number of carbon atoms at the alkyl side chain derived from alcohol. For convenience, this sample ID will be used through out the paper. The lengths of the geometry optimized structures of these carbamates, calculated using HyperChem Pro 6 molecular visualization and simulation software, are also listed in Table 1.

Preparation of Blends. Binary blends of carbamates were prepared by melt mixing, with 80/20, 60/40, 50/50, 40/60, and 20/80 (wt %) compositions. Preweighed mixtures of carbamates were heated in a 10 mL beaker at 120 °C with continuous stirring. After 1 h, the melt was slowly cooled to room temperature. Three types of binary blends were prepared, with C_{12}/C_{16} (see Table 1 for sample identification), C_7/C_{16}, and C_4/C_{16}. The first series was used for most of the study. The other two were used to rationalize the miscibility behavior.

Methods for Structure and Morphology. Thermal analysis was performed using a DuPont 910 differential scanning calorimeter at a heating rate of 10 deg/min. The instrument was calibrated for temperature and energy with indium and tin reference samples. DSC traces were recorded with about 7−10 mg of sample, in a nitrogen atmosphere.

X-ray diffraction data were collected within the range $2° \leq 2\theta \leq 50°$ with a Philips automated powder diffractometer, model PW 1710. Nickel-filtered Cu Kα radiation ($\lambda = 1.542$ Å) was used at 40 kV and 40 mA. The possible presence of texture was checked by taking additional diffractograms with samples turned in the plane of measurement by 90°. The MDI Datascan 3.2 software (Materials Data Inc., Livermore, CA) was used for data collection. The results were analyzed with MDI Jade 5.0 XRD pattern processing software. Percent crystallinity of the sample, Xc, was calculated using the formula

$$\text{Xc} = (\text{crystalline area under the peak}/\text{total crystalline and amorphous area}) \times 100 \quad (1)$$

The crystallite size, L, corresponding to a particular reflection was calculated by the Scherrer equation:[15]

$$L = K\lambda/\beta \cos\theta \quad (2)$$

where λ is wavelength of the X-ray, θ is half the scattering angle, and β is the half width of the peak on the 2θ scale in radians; $K = 0.9$.

Considering the molecular length of the carbamates, significant X-ray reflections were expected at $2\theta < 5°$ ($d > 17.7$ Å). The diffraction patterns obtained below 5° by the above diffractometer were not reliable; i.e., the peaks were not well-resolved because of overlap with the background. Hence, additional diffraction patterns were recorded under vacuum with a Statton-type Warhus flat film camera (William Warhus Co., Wilmington, DE), using Cu Kα radiation ($\lambda = 1.542$ Å), with sample to film distances of 10 and 17 cm.

The optical micrographs were recorded on a Zeiss Axioplan polarized optical microscope (OM), equipped with a Linkam hot stage. Northern Eclipse (version 6.0) image processing software was used to capture the images as well as to calculate the spherulite size (where it was possible). The samples for optical microscopy were prepared by melting a small amount of the material on the microscope slide at a temperature 20 °C higher than its melting point, holding it isothermally for 10 min to remove any morphological history, and then cooling it down slowly to room temperature at the rate of 10 deg/min. Another set of samples was prepared following the same procedure, but this time the samples were quenched from the melt, instead of slow cooling.

Small-angle light scattering (SALS) was used primarily in the H_v mode to detect the spherulitic crystalline morphology. This technique involves the photometric measurement of the scattered intensity, which arises mainly from fluctuations in anisotropy in the crystalline domains, as a function of scattering angle. The setup described by Jabarin and Stein,[16] includes a 10-mW He−Ne laser with $\lambda = 0.6328$ μm, a rotatable analyzer, and a photographic setup for Polaroid 4×5 Land film. The vertically polarized incident laser beam was passed through a 2-mm pinhole to avoid stray radiation and the pattern was recorded with the optical axis of the analyzer kept horizontal (H_v mode). The average size of the spherulite is given by[17]

$$4\pi(R/\lambda)\sin(\theta/2) = 4 \quad (3)$$

with

$$\theta = \tan^{-1}(r/D) \quad (4)$$

Here R is the radius of the spherulite, λ is the wavelength of the laser beam, r is the distance on the H_v photograph from the center of the incident beam to the point of maximum intensity on the four-leaf clover pattern, and D is the sample to film distance.

Results and Discussion

Optical Microscopy. The spherulitic morphology depends on the length of the alkyl chain as well as whether the sample was slowly cooled or quenched. The slow cooled and the quenched samples of C_4 showed spherulitic morphology (Figure 1a,a′) with a classical Maltese cross. They exhibited negative birefringence indicating that the crystallites are oriented tangentially within the spherulite.[18] The intensity of the birefringence was low. The samples of C_7 and C_8 (Figure 1b,b′) also showed similar negatively birefringent spherulites. While the Maltese cross was well-defined in the quenched samples of C_7 and C_8, it was not with the slow-cooled sample. On the other hand, the slow-cooled samples of C_{12} showed highly coarsened spherulites with *positive* birefringence (Figure 1c). It is likely that in these spherulites also the crystallites grow in a tangential direction (as in normal negative spherulites) but many branches

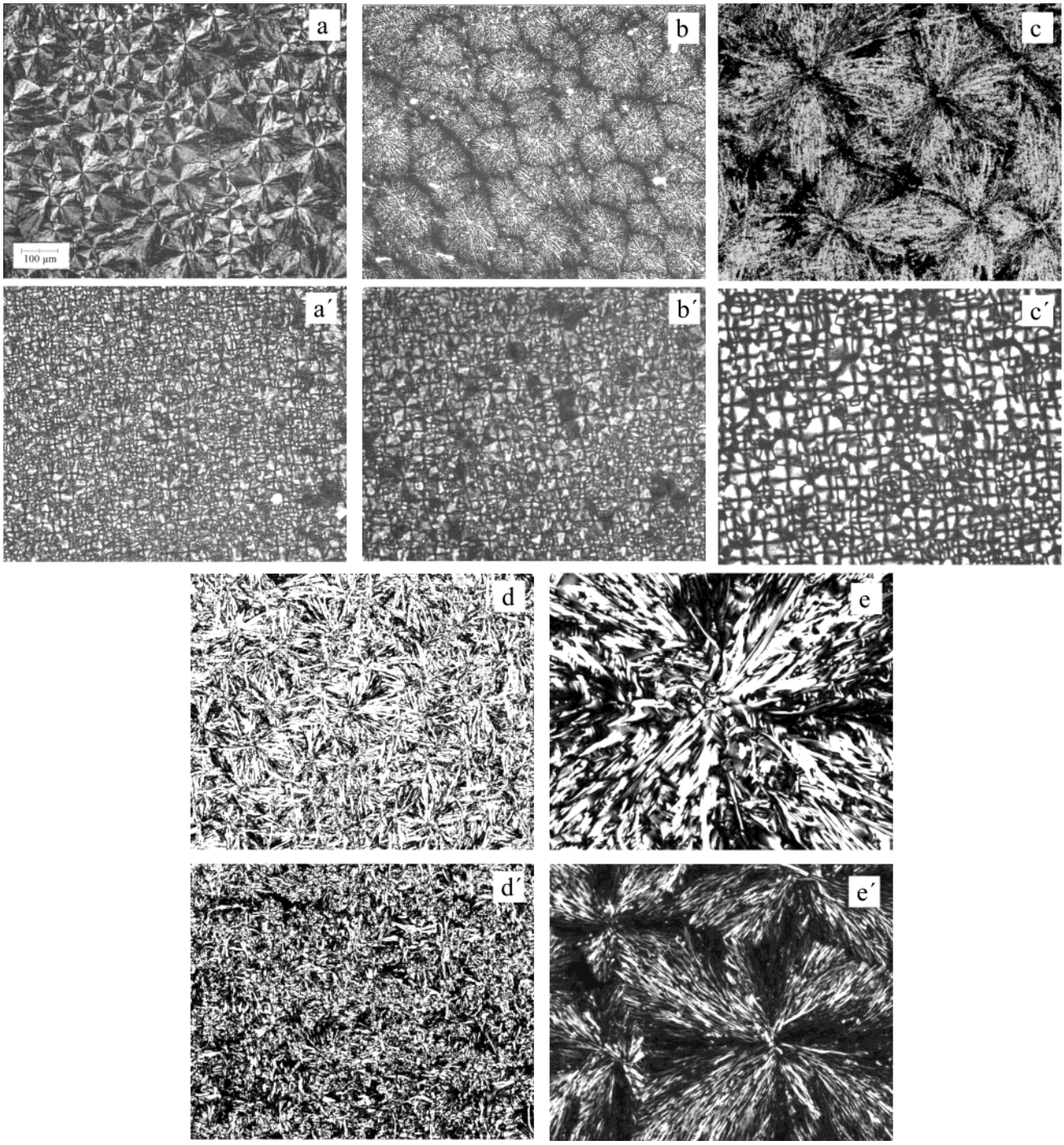

Figure 1. Optical micrographs of different carbamates: slow-cooled samples of C_4, C_8, C_{12}, C_{16}, and C_{18} respectively a−e; quenched samples of C_4, C_8, C_{12}, C_{16}, and C_{18} respectively a′−e′.

grow perpendicularly to this principal growth direction, exhibiting positive birefringence.[18] Another interesting feature is that these spherulites showed a Maltese cross at 45° to the polarizing direction, which is characteristic of an unusual type of spherulite. (Note that in Figure 1c′, the extinction is along the vertical and horizontal directions of the page, while it is at an angle of about 45° in Figure 1c.) This unusual type is a characteristic of spherulites whose optical axis lies at an angle of approximately 45° to the spherulitic axis.[19−21] The quenched sample of C_{12} still exhibited positive birefringence, but the Maltese cross was found to appear along the polarizers (0° and 90°) (Figure 1c′), indicating that the optic axis is now parallel to the spherulite axis. The slow cooled and quenched samples of C_{16} exhibited needle-shaped crystals (Figure 1d,d′). In most cases, these crystals were found to aggregate surrounding a center. Slow cooled and quenched samples of C_{18} formed fibrillar spherulites with negative birefringence (Figure 1e,e′). Thus, only the C_{12} sample showed positive birefringence and unusual type of spherulites. But for this, there was no effect seen due to the odd−even nature of the alkyl chains or the asymmetry of the chains on either side of the −NHCOO− group on the birefringence. However, progressive fibrillation is seen with an increase in the length of the alkyl chain.

The spherulites from the slow-cooled and the quenched samples were large enough to measure their radius from the optical micrographs. The spherulite size increases gradually from C_4 to C_{12} and then there is a sharp increase of spherulite size for C_{18} (Figure 2). The size of the spherulites decreases

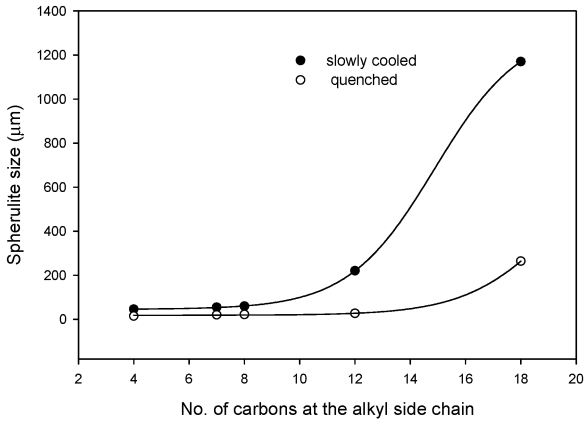

Figure 2. Spherulite size as a function of number of carbons at the alkyl side chain derived from alcohol.

significantly when the samples were quenched instead of slow cooled. For example, when C_{18} was slowly cooled from the melt, the average spherulite size was 1170 μm, whereas in the quenched sample, it decreased to 220 μm.

Blending affects the morphology significantly, as expected. The 80/20 blend of C_{12}/C_{16} showed tiny spherulites under the optical microscope (Figure 3a). With an increase in the fraction of C_{16}, the blends showed a mixture of crystals, some of which were needle shaped while the others were spherulitic (Figure 3b,c). These can be compared with the micrographs exhibiting large spherulites for the individual components, shown in Figure 1c,d. The spherulites in the blends exhibited very low birefringence. The sign of the birefringence could not be determined. In most cases, the size of the spherulites was not large enough to determine reliably from the optical microscope, but small-angle light scattering could be used in some cases. It is noteworthy that the transparency of the 80/20, 60/40, and 50/50 blends was found to improve significantly as compared to that of pure C_{12} or C_{16}.

Small Angle Light Scattering. The H_v scattering patterns were recorded with the same sample−film distance. Those arising from spherulites of slow-cooled samples of C_4, C_7 and C_8 showed the characteristic four-leaf clover pattern, having 45° intensity maximum.. The slow cooled sample of C_{12} showed intensity maximum at 0° and 90° (Figure 4a) but the quenched sample showed the more common 45° intensity maximum (Figure 4b). This is consistent with the observation in the optical microscope: the observed H_v scattering pattern for the slow-cooled sample of C_{12} is characteristic of the spherulite having an angle between the optic axis and the spherulite axis. Both the slow-cooled and quenched samples of C_{16} also exhibited an H_v pattern with intensity maxima at 0° and 90°, i.e., the unusual type. However, C_{18} exhibited the usual four-leaf clover pattern. Figure 5 shows the H_v patterns obtained from the slow-cooled samples of the blends of C_{12} and C_{16} at different compositions. The four-leaf clover pattern was found to become larger with increasing incorporation of C_{16} in the blend, indicating a decrease in the size of the spherulites. As seen in Figure 6, the size of the spherulites in the blend calculated from the SALS pattern decreases with an increase in the fraction of C_{16} (Figure 6). This decrease in spherulite size can be attributed to the heterogeneous nucleation and less ordered state of the blend compared to the pure materials. Thus, the effect of blending these two carbamates is similar to the role of clarifiers to reduce the spherulite size. As mentioned above, the transparency of the films improves significantly with the blends. The four-leaf clover patterns obtained from the quenched samples of the blends were not perfect, probably due to the size of the spherulites being too small. Hence, they were not used to calculate the spherulite size.

Thermal Analysis. The melting points of the carbamates obtained from DSC are shown at Table 1. In all the carbamates, only one phase transition from solid to liquid was observed. This indicates the absence of any detectible impurity or any polymorphic transition prior to melting. There was a linear increase of the melting point with the increase of the alkyl side chain. The melting point of the slow-cooled and the quenched samples did not differ significantly. Heat of fusion data showed sigmoidal characteristics as the length of the alkyl side chain increases. Up to C_{12}, the heat of fusion did not increase much, but after that it increased linearly. The heat of fusion of the slow-cooled samples was found to be higher than that of the

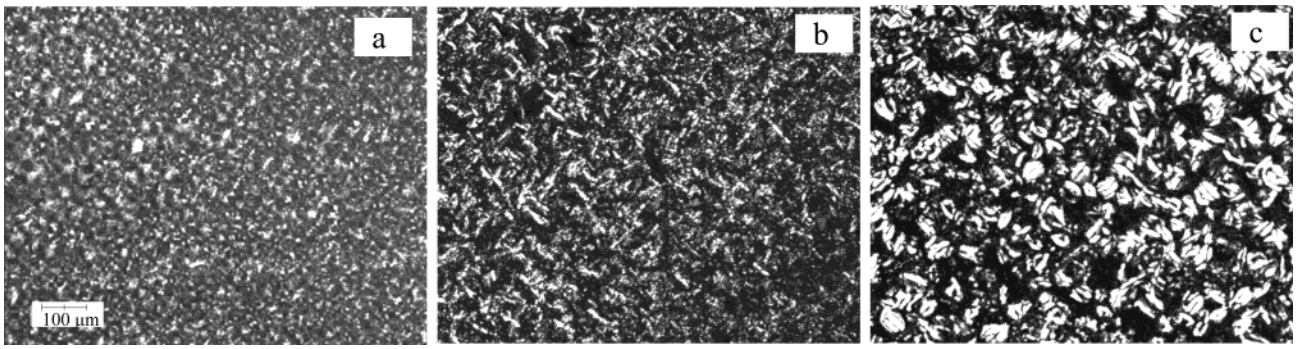

Figure 3. Optical micrographs of the slow-cooled samples of C_{12}/C_{16} blends (a) 80/20, (b) 60/40, and (c) 50/50.

TABLE 2: Melting Points of Binary Blends of Carbamates

C_{12}/C_{16}		C_7/C_{16}		C_4/C_{16}	
sample	melting point/s, °C	sample	melting point/s, °C	sample	melting point/s, °C
100/0	72.8	100/0	65.5	100/0	61.2
80/20	69.5	80/20	62.7	80/20	58.2
60/40	68.9	60/40	62.4	60/40	57.5, 67.1
50/50	68.5	50/50	62.1, 72.2	50/50	57, 69.6
40/60	67.2, 73.8	40/60	61.7, 74.7	40/60	57, 72.7
20/80	65.5, 78.7	20/80	60.6, 79	20/80	56.4, 72.7
0/100	83	0/100	83	0/100	83

TABLE 3: Interplanar Spacings *d* (Å) and Relative Intensities (%) of X-ray Diffraction Maxima for the Various Carbamates

C_4		C_7		C_8		C_{12}		C_{16}		C_{18}	
d	I	d	I	d	I	d	I	d	I	d	I
42.5	m	42.6	m	42.8	m	64.7	m	62.4	m	64.7	m
29.9	m	33.4	m	35.1	m	51.4	w	52.1	m	52.4	m
26.8	m	30.2	m	31.6	m	44.7	m	46.1	m	46.4	m
24.5	100 (s)	28.1	100 (s)	29.4	100 (s)	39.6	m	42.3	m	42.3	m
14.2	w	20.9	39.7	22.6	39.0	32.0	100 (s)	35.9	100 (s)	38.1	100 (s)
13.5	w	16.4	w	15.6	w	23.7	23.7	20.6	30.2	26.9	35.8
12.1	36.8	15.3	m	14.3	18.0	16.2	10.0	13.3	m	22.4	w
8.84	w	13.8	21.6	9.1	w	13.3	m	12.1	13.9	19.1	w
8.02	12.4	11.5	w	7.12	9.7	12.0	m	10.6	w	14.8	w
4.96	m	9.8	w	5.67	6.4	10.6	8.3	9.82	m	14.0	w
4.63	w	9.1	w	4.94	9.0	7.93	6.9	7.25	6.1	13.0	m
4.44	74.9	6.88	7.7	4.61	M	5.24	5.6	4.41	43.5	12.5	16.5
4.24	w	5.49	w	4.44	58.8	4.67	18.3	4.29	m	10.4	m
4.03	30.8	4.97	8.5	4.26	m	4.52	19.5	4.18	15.7	9.20	w
3.84	61.3	4.60	w	4.01	w	4.29	37.8	4.05	w	7.94	w
3.66	38.3	4.44	62.0	3.87	86	4.05	w	3.90	81.7	7.52	6.7
3.46	w	4.21	20.2	3.56	26.1	3.91	58.1	3.64	33.1	5.37	4.2
		4.01	m	3.25	8.5	3.77	26.5			4.93	w
		3.88	80.1			3.61	17.0			4.66	w
		3.69	m			3.50	9.3			4.44	35.8
		3.54	20.5			3.33	6.2			4.28	m
		3.36	w							4.16	9.4
		3.23	w							4.00	w
										3.89	45.6
										3.68	w
										3.58	20.3
										3.17	4.1

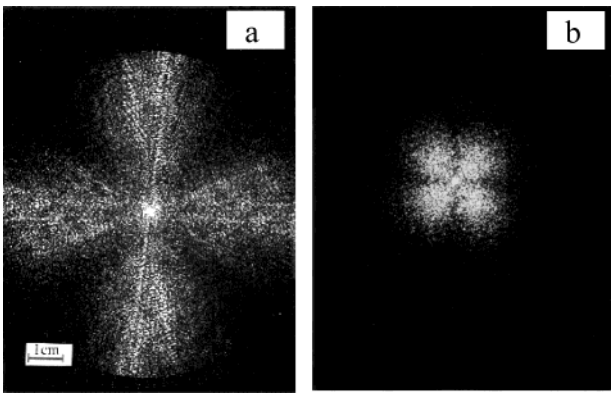

Figure 4. H_v scattering pattern for C_{12} (a) slowly cooled and (b) quenched. The sample−film distance is the same in this figure and in Figure 5.

quenched samples, consistent with the X-ray crystallinity measurements.

Let us now consider the thermal characteristics of the blends. Figure 6 shows the heat of fusion as a function of the blend composition for the binary blends prepared from C_{12} and C_{16}. It is seen that initially there is a decrease in the heat of fusion with the incorporation of C_{16} in the blend. It passes through a plateau at the weight fraction of 0.4 of C_{16} and then increases significantly with an increase in the content of C_{16}. A similar behavior was found with the C_4/C_{16} and C_7/C_{16} blends. In all these cases, the heat of fusion of the slow-cooled samples is higher than that of quenched samples.

If the heat of fusion shows such variations with the blend composition, the question arises as to the miscibility of the components in the blends: whether the two carbamates cocrystallize leading to a structure with poor crystallinity or one acts as a plasticizer for the other. If the two components were miscible, we would expect a single melting point, intermediate between those of the individual components. The components in the blend are of a homologous series; they both have hydrogen-bonding segments and alkyl chains. The DSC thermographs of the blends of C_{12} and C_{16} are shown in Figure 7. These are shown in three diagrams in order to provide clarity. It is seen from Figure 7a that 80/20 and 60/40 blends of C_{12} and C_{16} show a single peak in DSC ,indicating the possibility that they are miscible with each other. However, it is seen not to be the case, as discussed below. The 50/50 blend still shows

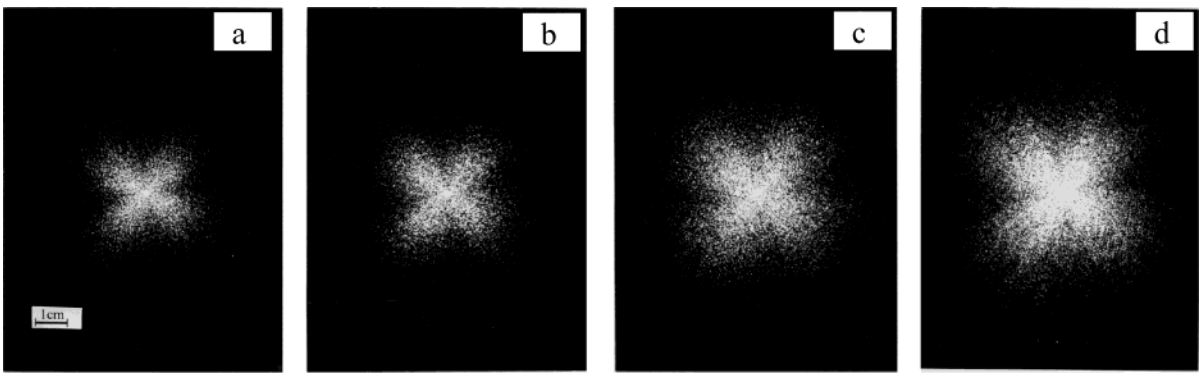

Figure 5. H_v scattering pattern for blends of C_{12}/C_{16} at composition of (a) 80/20, (b) 60/40, (c) 50/50, and (d) 40/60; all the samples are slowly cooled.

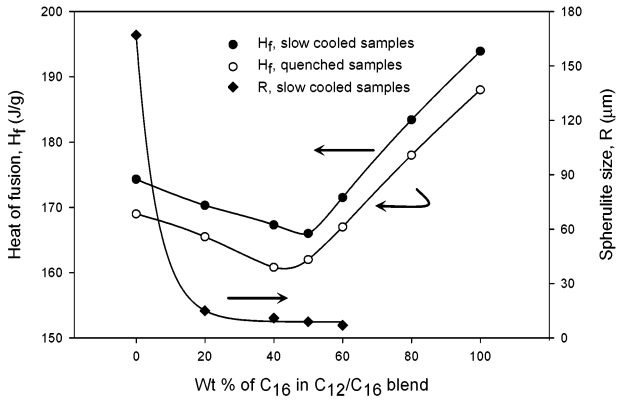

Figure 6. Spherulite size and heat of fusion as a function of weight percent of C_{16} in the binary blends of C_{12} and C_{16}.

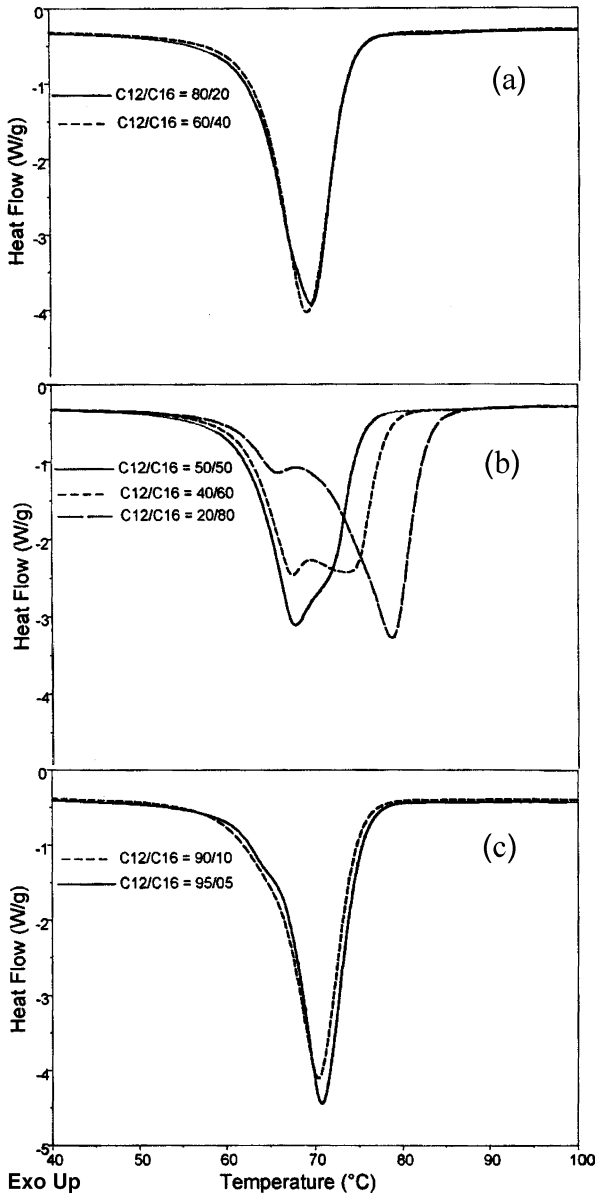

Figure 7. DSC thermographs of binary blends of C_{12}/C_{16} at (a) 80/20 and 60/40, (b) 50/50, 60/40, and 20/80, and (c) 90/10 and 95/05 compositions.

a single peak with a shoulder and broadening of full width at half-maximum (Figure 7b), but splitting of peaks occurs with 40/60 and 20/80 blends.

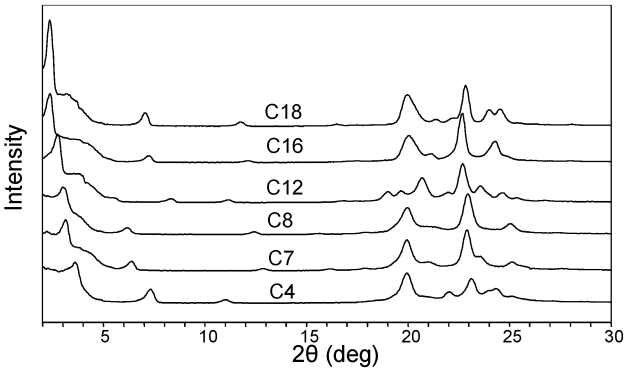

Figure 8. X-ray diffraction patterns of different carbamates.

The melting points of blends of different compositions of C_{12} and C_{16} along with the melting points of the pure carbamates are summarized in Table 2. Note that the melting temperature of C_{16} is higher than that of C_{12} by about 10 deg. Surprisingly, although the 80/20 and 60/40 blends of C_{12} and C_{16} exhibited a single peak in DSC, their melting points were found to be less than the melting point of pure C_{12}. If the single peak in 80/20 and 60/40 blends were due to the complete miscibility of C_{12} and C_{16} at these compositions, we would expect the melting point of the blends to be between the melting points of the components. To examine this anomaly, another two series of blends were prepared with C_{16}, but with C_4 or C_7 as the other member, to see its effect on the melting points of the blends. The difference in the lengths of the alkyl chains is large in the blend of C_{16} and C_4. The C_{16}/C_7 blend provides an example of mixing even−odd components. The results are summarized in Table 2.

Table 2 shows that when there was a splitting in DSC thermograms of the AB blends (A denotes the carbamate with shorter alkyl side chain), two melting points were observed; the first melting point was lower than that of pure carbamate A, and the second one was lower than that of pure carbamate B. As the fraction of A was decreased in the blend, the second melting point increased, whereas the first melting point decreased. From these observations, it seems that the carbamates A and B exert a mutual plasticizer effect on each other in the blend, resulting in a depression of melting points of both. At high concentrations of A, it depresses the melting point of B to such an extent that these two melting peaks overlap, resulting in one peak.

If this rationale is valid, a further increase of the amount of A in the blend should either give a single peak (because of overlap) or depress the melting point of B to such extent that the melting peak of B should be at a position lower than that of A. To confirm this, two binary blends with 90/10 and 95/5 compositions were prepared from C_{12} and C_{16}. Their DSC thermograms are shown in Figure 7c. There is still a single peak observed for the 90/10 composition. With 95/05 composition of C_{12} and C_{16}, a shoulder below the melting point of C_{12} was observed, which indicated that the single peak at some compositions was not due to miscibility but to the mutual plasticizer effect of the carbamates.

X-ray Diffraction. The X-ray diffraction patterns of different carbamates are presented in Figure 8 and the *d*-spacings and relative intensities are listed in Table 3.

It is seen from Figure 8 that all the carbamates exhibit the most intense peak below $2\theta = 5°$ ($d > 17.7$ Å). No significant diffraction maximum was observed at $2\theta > 30°$ ($d < 2.97$ Å). Some diffraction maxima below 5° were not well-resolved and in those cases the *d*-spacings were calculated from the pattern

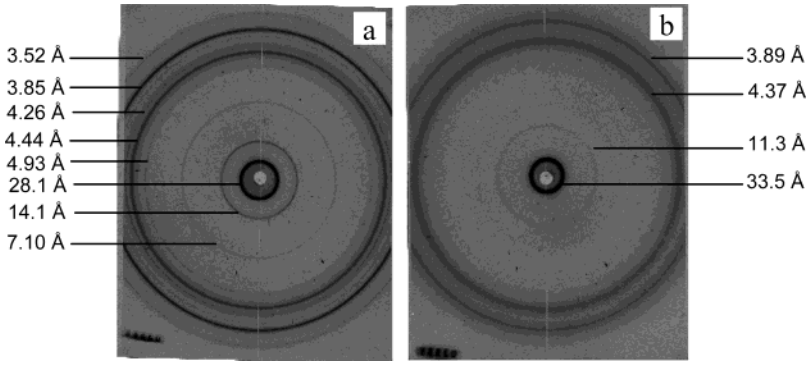

Figure 9. Diffraction patterns obtained from (a) C_8 and (b) 80/20 blend of C_{12}/C_{16}. The *d*-spacings are marked.

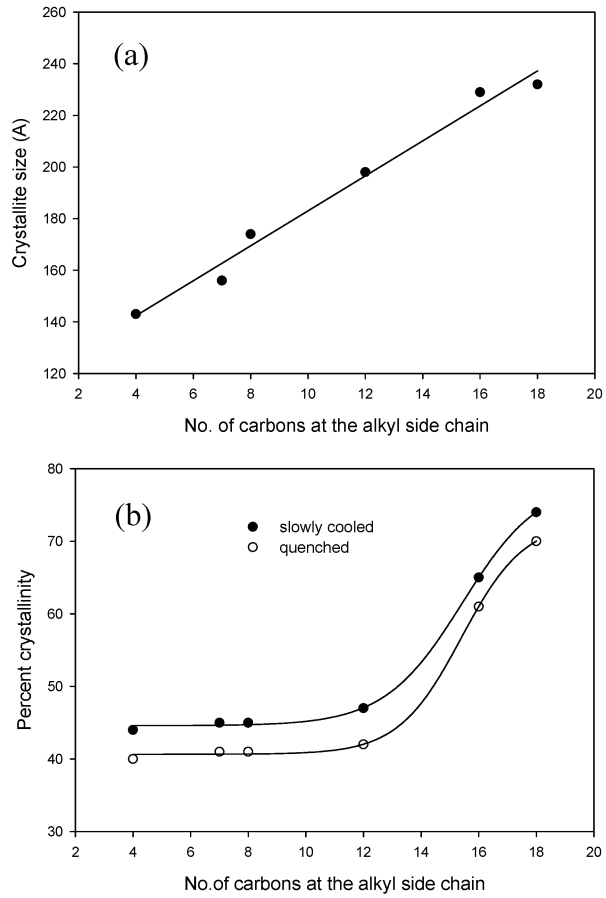

Figure 10. (a) Crystallite size corresponding to the reflection at 22.8° and (b) crystallinity as a function of number of carbon atoms at the alkyl side chain derived from alcohol.

recorded on film and their intensity is reported in Table 3 in terms of strong (s), medium (m), and weak (w). As an illustration, Figure 9a shows the diffraction pattern obtained from C_8.

Although it is not our intent here to determine the crystal structure of these carbamates, some general observations could be made from the diffraction data. Table 3 shows that the *d*-spacing of the most intense peak increases with the length of the alkyl side chain, from 24.5 for C_4 to 38.1 Å for C_{18}. The patterns recorded on film also show reflections with much larger spacings. The largest spacing recorded for C_4, C_7, and C_8 is about 42.5 Å, and this reflection does not show variation with the length of the alkyl side chain. Similarly, the reflection with a spacing of 62 Å does not show a systematic variation between C_{12}, C_{16}, and C_{18}. A medium intensity reflection with *d*-spacing corresponding to the molecular length was observed for all the carbamates (see Table 1).

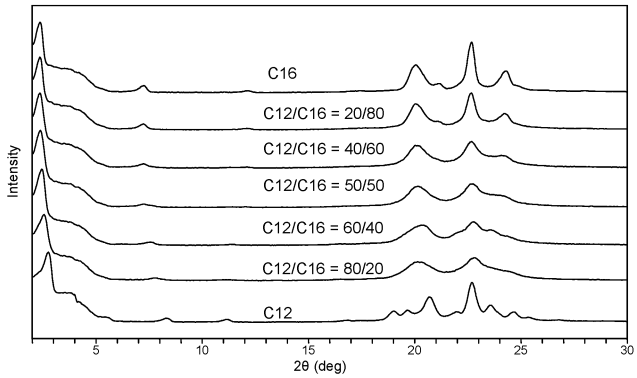

Figure 11. X-ray diffractograms of the binary blends of C_{12}/C_{16} along with those of C_{12} and C_{16}.

In all the diffractograms, there is a strong diffraction maximum at $2\theta \cong 22.8°$ ($d = 3.9$ Å). Using HyperChem simulation software, two molecules of, e.g., C_{18} were placed in proximity and the energy minimized. With the hydrogen bond between the two molecules, the distance between the alkyl chains was found to be 3.9 Å. Thus, the above *d*-spacing corresponds to the plane of hydrogen bonding. The crystallite size corresponding to this diffraction maximum was calculated for these carbamates, and the results are shown in Figure 10a as a function of the alkyl side chain length. The crystallite size is found to increase linearly with the increase of the length of the alkyl side chain. Figure 10b illustrates the crystallinity calculated from the X-ray diffractograms as a function of the number of carbons at the alkyl side chain derived from alcohol. Like the heat of fusion, the plot of X-ray crystallinity showed a sigmoidal characteristic. The crystallinity increases significantly only after C_{12}. In all cases, the crystallinity of the slow-cooled samples was found to be higher than that of quenched samples.

Figure 11 presents the X-ray diffractograms of binary blends of C_{12} and C_{16} along with the diffractograms of the pure carbamates. These diffractograms show several characteristics. At 80/20 composition of C_{12} and C_{16}, there is a reduction of number of peaks. The relative intensity of most of the peaks reduces compared to C_{12}. For example, the intensity of the diffraction maximum at $2\theta \cong 22.8°$, relative to the most intense peak, reduces from 58 to 37%, the full width at half-maximum (fwhm) increases from 0.366 to 1.108 rad on the 2θ scale, and the crystallite size decreases from 230 to 73 Å. With the possibility that reduction of peak in the 80/ 20 blend might be simply because the instrument was not sensitive enough to record some weak peaks, this diffractogram was compared with the diffraction rings obtained from the film X-ray as shown in Figure 9b. The film shows several additional peaks with very low intensity. The decrease in crystallite size is

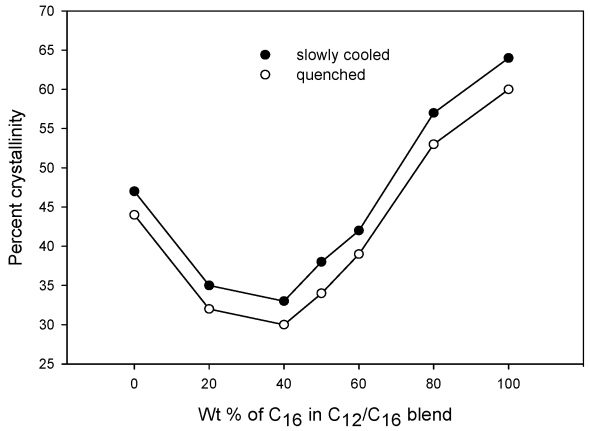

Figure 12. Percent X-ray crystallinity as a function of weight percent of C_{16} in the binary blends of C_{12} and C_{16}.

supported from the broadening of diffraction rings in Figure 9b. As the fraction of C_{16} increases in the blend, the relative intensity of the peaks gradually increases. However, for all the blends, the crystallite size corresponding to the reflection at $2\theta \cong 22.8°$ was found to be significantly lower than those of pure C_{12} and C_{16}.

Figure 12 shows the X-ray crystallinity as a function of the blend compositions. As shown in the figure, there is a decrease in the X-ray crystallinity with the incorporation of C_{16} in the blend. It passes through a plateau at the weight fraction of 0.4 of C_{16}, similar to the heat of fusion shown in Figure 6. Again the crystallinities of the slow-cooled samples were found to be higher than that of quenched samples.

The question arises as to whether the decrease in the crystallinity of the blend can be attributed to the disruption of the hydrogen bond, leading to less efficient self-assembly and the less ordered state of the blend compared to the pure carbamates. FTIR spectra of all the carbamates studied here showed bands at 1686 and 3337 cm^{-1} corresponding to hydrogen-bonded C═O and N—H stretching vibrations, and there was no absorption peak corresponding to free C═O or N—H. Thus all the C═O and N—H groups are hydrogen bonded. Another interesting aspect is that neither the frequency nor the intensity of the bands showed any change in the case of the blends, indicating that the extent of hydrogen bonding is unaffected by blending. However, it is seen above that the crystallinity, crystallite size, and spherulite size decrease with blend compositions. It was also discussed above that the components in the blends act as mutual plasticizers, depressing the melting point, and that they are not miscible. Thus, the changes in the morphology are caused by the differences in the packing of the alkyl chains in the blends, rather than by the disruption of the hydrogen bonds.

Conclusions

It was found that the length of the alkyl side chain of the carbamates has an influence on the morphology, heat of fusion, crystallinity, and crystallite size. Most of the long-chain carbamates exhibit spherulitic morphology; the size of the spherulites increases with the increase of the length of the alkyl side chain. Most of the carbamates exhibit negative birefringence, indicating the tangential orientation of chains within the spherulite. While the melting point increases linearly, the heat of fusion and crystallinity shows a sigmoidal trend. The crystallite size corresponding to the diffraction maximum along the hydrogen-bonding plane increases linearly with the increase of the alkyl side chain length.

The morphology can be controlled by the cooling rate as well as by blending. The crystal/spherulite size, heat of fusion, and crystallinity of the slow-cooled samples are higher than those of quenched samples. In some cases cooling rate can alter the optic axis with respect to the spherulite axis. Blending reduces the crystal/ spherulite size, heat of fusion, and crystallinity. Blending also improves the transparency of the sample significantly.

The carbamates exert a mutual plasticizer effect in the blend, resulting in the depression of melting point of the parent compounds. The single point at some compositions of the blend is probably due to the overlap of the two peaks rather than due to the miscibility of the parent compounds. This work shows the dependence of morphology and related properties on the structure of the carbamates and the blend compositions. It is interesting that blending of any two of the carbamates does not affect the self-assembling process itself, as indicated by the absence of any change in the IR spectra. Thus the morphological changes upon blending are not due to the disruption of the hydrogen bonds but are due to the poor packing of the alkyl chains. This shows that one could control the morphology of a self-assembling system by tailoring alkyl segments and without reducing the extent of the hydrogen bond network.

As mentioned in the Introduction, it is a common practice to use clarifiers as nucleating agents to control the morphology. We have shown here that blends of like molecules could be used for the same purpose. Although it is difficult to assess, due to the proprietary nature, if such blends are used currently in printing inks, there are examples in the patent literature to this effect.[22]

Acknowledgment. This work was supported by the Natural Sciences and Engineering Research Council of Canada (NSERC) and Xerox Research Centre of Canada (XRCC). M. Moniruzzaman was partly supported by the Ontario Graduate Scholarship for Science and Technology (OGSST).

References and Notes

(1) Steichele, K. Belg. Patent 882,922, 1980. *Chem. Abstr.* **1980**, *94*, 66768d.
(2) Saka, K.; Noda, K. Jpn. Kokai Tokkyo Koho JP 62 179 584, 1987; Chem. Abstr. **1987**, *108*, 39820r.
(3) Tanaka, K.; Kano, Y.; Yoshida, K. Jpn. Kokai Tokkyo Koho JP 63 248 894, 1988. Chem. Abstr. **1988**, *110*, 79137w.
(4) Kinoshita, H.; Sekiya, M.; Mishima, M. Eur. Pat. EP 274 756, 1988; Chem. Abstr. **1988**, *109*, 233979k.
(5) Kochansky, J.; Cohen, C. F. *J. Agric. Ent.* **1990**, *7*, 293.
(6) Jpn. Kokai Tokkyo Koho JP 58 201 758, 1983; Chem. Abstr. **1983**, *100*, 174289z.
(7) Tanaka, T.; Yoshitomi, T.; Hanada, Y.; Ohashi, M.; Takeda, Y. Jpn. Kokai Tokkyo Koho JP 6 290 289; Chem. Abstr. 107, 20896b.
(8) Goodbrand, B.; Boils, D.; Sundararajan, P. R.; Wong, R.; Malhotra, S. U. S. Patent 6,187,082, 2001.
(9) Furer, V. L. *J. Mol. Struct.* **1992**, *56*, 43.
(10) Furer, V. L. *J. Mol. Struct.* **1998**, *449*, 53.
(11) Furer, V. L. *J. Mol. Struct.* **1999**, *513*, 1.
(12) Furer, V. L. *J. Mol. Struct.* **2000**, *520*, 117.
(13) Deetz, M. J.; Jonas, M.; Malerich, J. P.; Smith, B. D. *Supramol. Chem.* **2002**, *14*, 487.
(14) Krol, P.; Wietrzynska-Lalak, Z. *Eur. Polym. J.* **1995**, *31*, 689.
(15) Alexander, L. E. *X-ray Diffraction Methods in Polymer Science*, 1st ed.; Wiley- Interscience: New York, 1969; p 335.
(16) Jabarin, S. A.; Stein, R. S. *J. Phys. Chem.* **1973**, *77*, 399.
(17) Stein, R. S.; Rhodes, M. B. *J. Appl. Phys.* **1960**, *31*, 1873.
(18) Bodor, G. *Structural Investigation of Polymers*, 1st ed.; Ellis Harwood Ltd.: New York, 1991; p 163.
(19) Stein, R. S.; Misra, A. *J Polym. Sci., Polym. Phys. Ed.* **1980**, *18*, 327.
(20) Stein, R. S. in *Structure and Properties of Polymer Films*; Lenz, R. W., Stein, R. S., Eds.; Plenum: New York, 1973.
(21) Park, C.-S.; Lee, K.-J.; Kim, S. W.; Lee, Y. K.; Nam, J.-D. *J. Appl. Polym. Sci.* **2002**, *86*, 478.
(22) Goodbrand, B.; Boils, D. C.; Sundararajan, P. R.; Wong, R. W. US Patent 6,414,051, 2002.